Spring 2024

Characterization of the Kansas river alluvial aquifer using towed transient electromagnetic geophysical method

Jonathon Daniel Voss
Missouri University of Science and Technology

CHARACTERIZATION OF THE KANSAS RIVER ALLUVIAL AQUIFER USING TOWED TRANSIENT ELECTROMAGNETIC GEOPHYSICAL METHOD

by

JONATHON DANIEL VOSS

A THESIS

Presented to the Graduate Faculty of the

MISSOURI UNIVERSITY OF SCIENCE AND TECHNOLOGY

In Partial Fulfillment of the Requirements for the Degree

MASTER OF SCIENCE IN GEOLOGICAL ENGINEERING

2022

Approved by:

Katherine Grote, Advisor
Ryan Smith, Co-Advisor
Jeremy Maurer

ABSTRACT

Forecasted urban development areas west of Kansas City, Kansas in the coming decades has caused an increase of research into water resources (Butler et al. 2022). A location of investigation has been the Kansas River Alluvial Aquifer (KRAA) for shallow ground water resources. To investigate the KRAA structure and grain texture, the towed transient electromagnetic system (tTEM) in conjunction with direct push electrical conductivity logs and lithology wells were used to investigate four locations between Lawrence and Manhattan, Kansas. In total, 110 line-kilometers of tTEM data was collected. The tTEM data collected were high quality and through inversions of the data were able to display resistivity information to a depth of investigation (DOI) of approximately 70 meters. To interpret these results, 31 local lithology wells were used to compare the tTEM data. From the lithology wells, three grain types were determined to be used for analysis: fine, medium, and coarse. Distributions of resistivity values for these grain textures were found by solving for resistivity values that match data from lithology well data most closely. Direct push electrical conductivity logs were used to validate the tTEM data, and the refusal depth of the lithology wells and direct push electrical conductivity were then used to characterize the bedrock with the tTEM results. Using inversion models and grain texture results, resistivity and grain texture profiles of the subsurface were developed covering a very large cross-sectional area. The methods implemented and developed in this study have increasing benefit of the deployment and analysis of tTEM data due to its low cost of deployment and the DOI the tTEM system can achieve in alluvial settings.

ACKNOWLEDGMENTS

The quality experience researching this material would not be possible without Dr. Ryan Smith, who is absolutely amazing. His vast knowledge and mentorship the past two years have been invaluable, and I am very thankful to have been his student.

I would also like to thank the Kansas Geological Survey not only for funding for this research but for the hospitality and knowledge they gave me when in the field with them.

I would finally like to thank my parents and my wife. Without the support of you, none of this would be possible.

TABLE OF CONTENTS

Page

LIST OF ILLUSTRATIONS

Page

LIST OF TABLES

Page

1. INTRODUCTION

1.1. GENERAL INTRODUCTION

Forecasted urban development areas west of Kansas City, Kansas in the coming decades has caused an increase of research into water resources (Butler et al., 2022). A location of investigation has been the Kansas River Alluvial Aquifer (KRAA) for near surface water resources. To investigate the KRAA structure and grain texture, the towed transient electromagnetic system (tTEM) in conjunction with direct push electrical conductivity (DPEC) and lithology wells were used to investigate four locations between Lawrence and Manhattan, Kansas.

1.2. PURPOSE AND SCOPE

The purpose of this study is to investigate subsurface properties in various location of the KRAA. This was accomplished by using the tTEM device to develop resistivity models through inversions to provide a large spatial resolution of the subsurface. The resistivity models could then be compared with local lithology data to create a soil texture map of the subsurface. The soil texture maps could then help characterize the locations of fine, medium, and coarse-grained materials. With these textures outlined, the overall structure of the KRAA could then be defined at the four survey locations. The results of the grain texture analysis could then be used to best estimate where water resources could be located within the KRAA.

1.3. THESIS ORGANIZATION

This thesis contains five sections. Section 1 contains the general introduction and motivation of the work. Section 2 contains the literature review related to the tTEM device and methods of utilizing tTEM data, as well as background information of the KRAA. Section 3 contains the methods of which the tTEM and DPEC data was collected, processed, and analyzed. Section 4 contains the results and discussion of the work. Finally, section 5 contains the conclusions and recommendations of the work.

2. LITERATURE REVIEW

2.1. tTEM REVIEW

The tTEM system is designed for highly efficient and detailed mapping of the shallow subsurface (Auken et al., 2019). The tTEM data helps fill gaps where well logs provide very limited spatial data. Detailed 3D geophysical and or geologic information of the shallow subsurface is commonly used to outline aquifer characteristics, groundwater vulnerability, regulation of land use, infrastructure development, artificial infiltration cases, surface and groundwater interaction, and other subsurface applications (Auken et al., 2019).

tTEM configuration consist of an all-terrain vehicle (ATV) pulling the tTEM transmitter and receiver while also carrying devices necessary for the tTEM operation. These devices consist of a battery, communications box, and computer. While surveying, the driver of the ATV also monitors the collection of the tTEM from a tablet that acts as the monitor to the computer. The transmitter (Tx coil) and receiver (Rx coil) are towed behind the ATV while collecting data. The Tx coil and Rx coil are mounted on sleds for smooth rides over fields and terrain. The sleds and frames of the Tx coil and Rx coil are built of a non-conductive fiberglass (Foged & Christiansen, 2020). The Rx coil is a 0.56 x 0.56 m multiturn coil, and the Tx coil is a 4 x 2 m rectangular coil (Auken et al., 2019). The small Tx coil makes ground transportation of the tTEM possible, while also large enough to capture a relatively large area while surveying. Figure 2.1 outlines the tTEM and its dimensions.

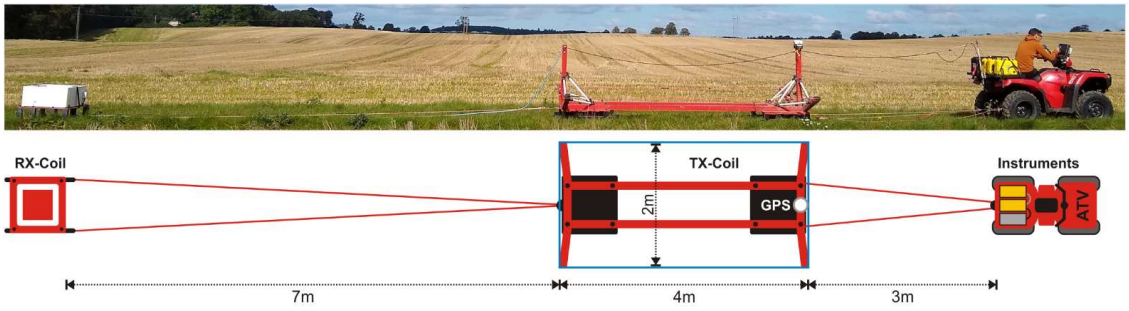

Figure 2.1 tTEM Dimensions (Auken et al., 2019).

The tTEM device operates by the following. The Tx coil produces a time-varying electrical current that is held at a steady state, which produces a static primary field, and is then abruptly turned off (Behroozmand et al., 2019). Once the transmitter is abruptly turned off, the change in the primary magnetic field induces an electromotive force in the ground that results in electrical eddy currents in the subsurface (Behroozmand et al., 2019). The eddy currents in the subsurface produce secondary magnetic fields. As time passes, the decaying secondary magnetic fields induce an electromotive force in the receiver coil (Behroozmand et al., 2019). The transient electromagnetic (TEM) signal is measured as a time derivative of the vertical component of the magnetic field (Behroozmand et al., 2019). The signal ranges over a few orders of magnitude in a very short time which contains the resistivity information of the subsurface (Behroozmand et al., 2019). The tTEM device uses a dual-transmitter moment measurement sequence to obtain early and late time TEM data (Auken et al., 2019). Early moment data collected is considered the low moment, where shallower depth data is collected. Late moment data is considered the high moment, where greater depth data is collected. Each moment collects data within fixed time intervals known as gates. A transient is measured after each

transmitter pulse, which is referred to as a sounding. This process can be observed in Figure 2.2, where (a) outlines where the current can be show turning on and off, (b) displays the induced electromagnetic force created by turning the current on and off, and (c) displays the transmitter capturing the secondary electromagnetic field (sounding) as well as the gates within the sounding.

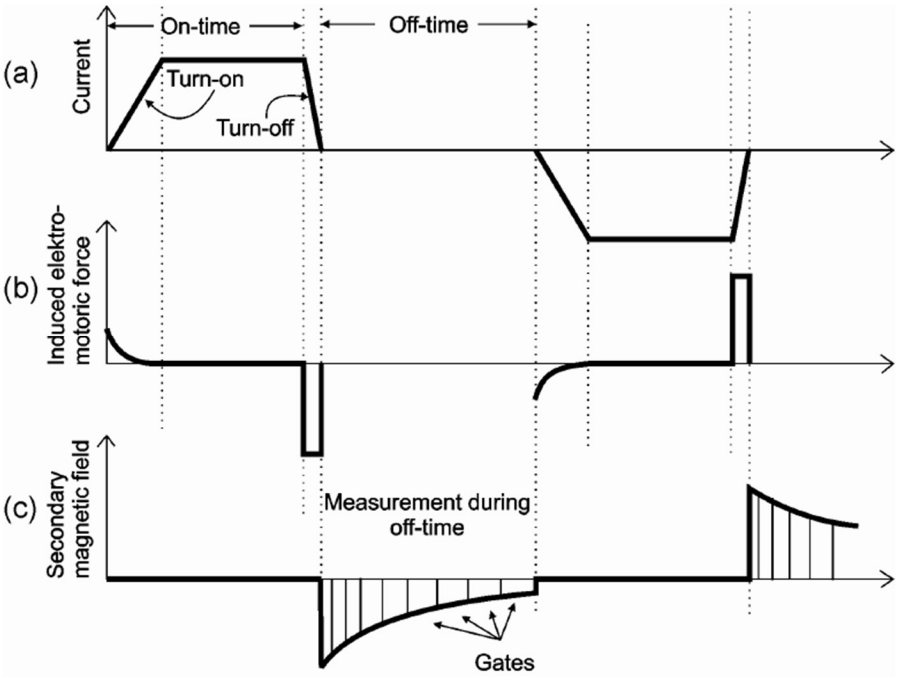

Figure 2.2 TEM Transmitted and Received Signal (Schamper et al., 2013)

Depth of investigation (DOI) is related to the signal to noise ratio (Auken et al., 2019). Typically, the target DOI of the tTEM is within the range of 0-80 meters. The tTEM does have the ability to map to depths of 120 meters where there the lack of conductive material is present. The DOI increases where there is a lack of conductive material as there is less signal lost to eddy currents. The DOI can also be extremely

shallow due to conductive material in the subsurface absorbing large amount of the signal created by the Tx coil. Because the tTEM is sensitive to conductive materials, conductive materials can be mapped with much higher confidence than non-conductive units. If a small non-conductive unit is contained within a large conductive unit, the small non-conductive unit will likely not appear in any data. Water content of the subsurface can also have a significant impact on the overall resistivity of the subsurface, which could affect the overall effectiveness of the tTEM (Goebel & Knight, 2021).

2.2. KANSAS RIVER ALLUVIAL AQUIFER

The main stem of the KRAA begins from Manhattan, Kansas to Kansas City, Missouri, where it joins the Missouri river. Most of the water available in areas surrounding the Kansas River come from the Kansas River and the groundwater from the KRAA (Whittemore et al., 2019). Projected population and economic expansion in this region in the coming decades will require pumping KRAA groundwater to help support expansion (Butler et al., 2022). Because of this, the state of Kansas has issued funding to better understand the KRAA structure (Butler et al., 2022).

The KRAA structure generally consists of alluvial deposits by the Kansas River. Quaternary alluvial deposits have the availability to extend from the near surface to bedrock in the region (~80 ft) and is underlain with Pennsylvanian to Permian age limestone and shale (Whittemore et al., 2019). In some regions, substantial alluvial deposits of sands and gravels can be found. The water table can also fluctuate greatly, where depths can range from near surface to 50 ft in depth (Whittemore et al., 2019). Because of the heterogeneity of these alluvial deposits, it can be difficult to best place

wells for high yield. Many wells placed in high yielding zones of large alluvial deposits may produce up to 1,000 gallons per minute (Whittemore et al., 2019). Figure 2.3 displays the general availability of groundwater and precipitation in Kansas, and outlines just how important the KRAA is to water availability in eastern Kansas.

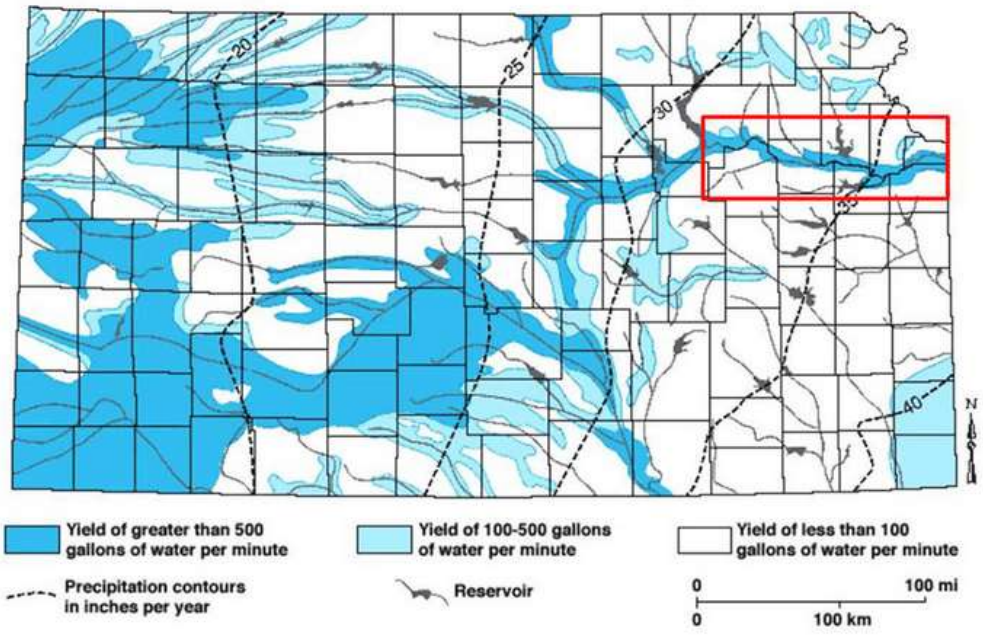

Figure 2.3 Groundwater Availability and annual precipitation in Kansas (Whittemore et al., 2019). The Kansas River Alluvial Aquifer is outlined in red.

2.3. ELECTRICAL RESISTIVITY LITHOLOGY RELATIONSHIP

The ability of geologic materials to conduct electricity varies to some degree based on grain size, minerology, and saturation, which makes data collected using the tTEM device interpretable to better understand local geology. Water content also plays a crucial role in the resistivity lithology results. Sediments with water in the pore space, the primary mechanism for electrical conduction (conductivity) is primarily ionic conduction

through the pore water (Knight et al., 2018). This results in a decrease of resistivity as the volume of water filled porosity increases (Knight et al., 2018). For the KRAA, the quality of the water is fresh, although it has a high carbonate concentration as the groundwater flows though calcareous bedrock underlying the aquifer and valley walls (Whittemore et al., 2019). Fortunately, high carbonate concentrations in groundwater do not reflect a high variation in groundwater conductivity, therefore this study assumes groundwater conductivity does not vary spatially. Because conductivity of the subsurface is primarily due to the ionic conduction through the pore water, it is expected to see higher resistivity values above the water table (Knight et al., 2018). General relationships in resistivity and lithology of various geologic materials have been established in literature but have extreme ranges that commonly overlap with other materials. Table 2.1 outlines materials with corresponding resistivity ranges expected to be found in the KRAA. For this research, a local variation of resistivity-lithology relationship was created using local well logs and tTEM results to obtain a more detailed understanding of the KRAA grain texture and structure.

Table 2.1 Possible Resistivity Lithology Ranges (Reynolds, 2011).

Geologic Material	**Resistivity (Ωm)**
Sand and Gravel	30 - 225
Sand clay / clayey sand	30 - 215
Clays	1 – 100
Consolidated shales	20 - 2000
Limestones	$50 – 10^7$

3. METHODS

3.1. GENERAL INTRODUCTION

In total four locations across the KRAA were surveyed. The total length of all surveys combined is 110 line-kilometers. The locations were chosen based on their distance apart from one another to create a generalized structure of the aquifer from Lawrence, Kansas to Manhattan, Kansas. The site names include RL01 at Manhattan, WB01 at Wamego, JF01 near Topeka, and DG02 at Lawrence. Figure 3.1 outlines the survey locations.

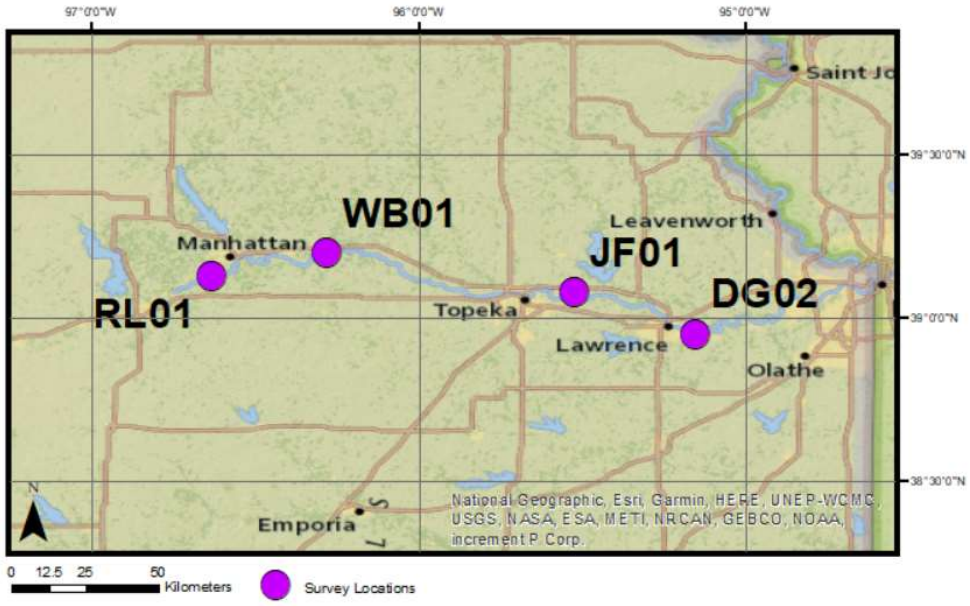

Figure 3.1 Survey Locations.

tTEM is very sensitive to electrical noise such as power lines and transformer stations. Locations with the best data collection are RL01 and WB01 due to the absence of electrical noise typically found in a large city. The location with the most electrical

noise is DG02 at Lawrence, as the survey was conducted close to the city creating the potential for large amount of noise resulting in more data being excluded in the analysis. The amount of data collected at locations depended on landowner approval, noise present at each location, and ability of the tTEM device to be towed over certain ground conditions. WB01 provided ample amount of data to be collected while JF01 had minimal landowner approval and difficult terrain.

3.2. tTEM DATA PROCESSING

Once all data was collected, editing and processing of the tTEM data began. The first step of data processing involves ensuring the gate signs are correct, filtered, and stacked (Auken et al., 2019). The gates are linearly spaced in logarithmic time to ensure sufficient time resolution in the early gates and optimum signal to noise at later gates (Auken et al., 2019).

The second process of data processing involved manually editing the raw data for any noise from metal objects, electrical noise, and mechanical noise. Metallic objects were rarely encountered in the survey but cause a mixing of gate data. Electrical noise was commonly encountered in locations close to large towns, specifically in the Lawrence area. Occasionally, the tTEM device was towed across rough surfaces, resulting in the receiver coil being exposed to mechanical noise in the form of vibrations and rotations (Auken et al., 2019). To remove the noise, processing of the raw change of the magnetic field with respect to time (dB/dt) data was conducted. Manual processing of tTEM data consists of a visual inspection of dB/dt data in a profile view (Foged & Christiansen, 2020). Automatic filtering of raw dB/dt data typically only detects and

removes heavily disturbed data (Foged & Christiansen, 2020). Manually filtering raw dB/dt data was done to ensure good data was used in later analysis. Figure 3.2 displays raw dB/dt data collected and visualized, where each colored line represents a gate in one sounding. Soundings are grouped as a combination of both a high and low moment at one time interval.

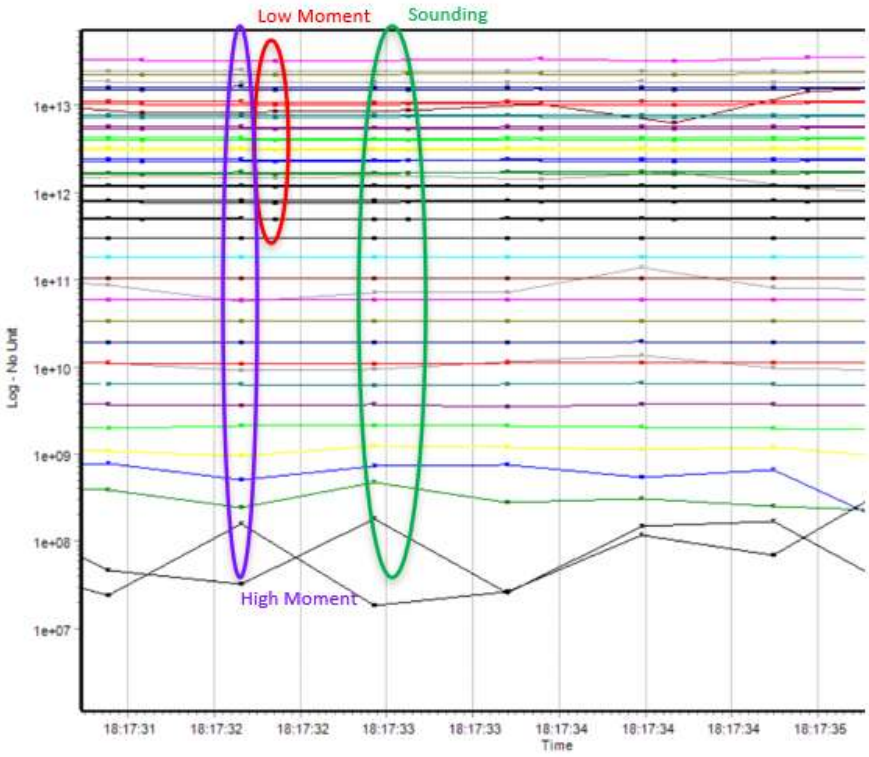

Figure 3.2 raw dB/dt data.

Once the noise was removed from the data, inversions of the tTEM data could be conducted to get final resistivity results. Both Spatially Constrained Inversions (SCI) and Laterally Constrained Inversions (LCI) were conducted with these data with an initial model of 40 ohm-meters that was iteratively varied to best fit the observed dB/dt data

until convergence was reached. The results of the LCI and SCI inversions in this study were had no significant differences. SCI data was used to continue with analysis due to the ability to obtain 2-D sky view resistivity maps, as well as exporting profile data for further analysis. SCI uses Delaunay triangulation to set 3-D constraints from well determined parameters to locally poorly determined parameters (Viezzoli et al., 2009). SCI provides more uniform and detailed results than maps obtained with the LCI inversion also used in this study (Viezzoli et al., 2009). SCI models at each location were completed successfully, with very low modeled residuals for each location. The DOI was determined to be at approximately 70 meters at the four locations, as the signal to noise ratio increased passed this depth and the inversion began to converge back to the initial 40 ohm-meter model.

A general 2-D resistivity profile was created for two locations following the data analysis from SCI models. A resistivity profile of DG02 was not created as the data was too coarse and in a non-linear position for a profile to be created, and a resistivity profile of JF01 was not created as the data was not perpendicular to the river and non-linear. The profile lines and data availability are shown in Figures 3.3 and 3.4 of WB01 and RL01. SCI sky view data availability of DG02 and JF01 are also included as Figures 3.5 and 3.6. SCI sky view rasters at each location are available in 1-meter intervals from 0-70 meters. These sky view rasters are beneficial in the amount of 2-D area they provide, which can be interpreted using the resistivity-lithology analysis.

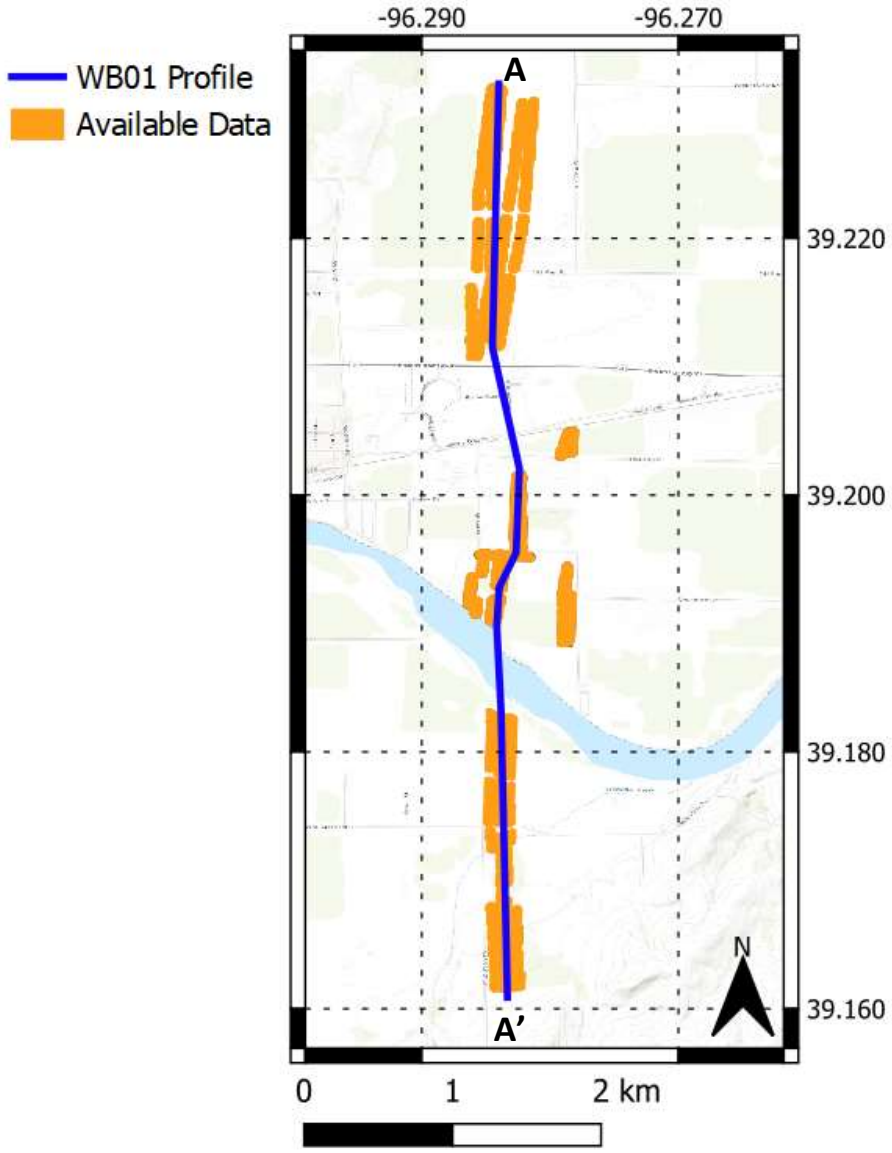

Figure 3.3 WB01 Available SCI data and Profile Line.

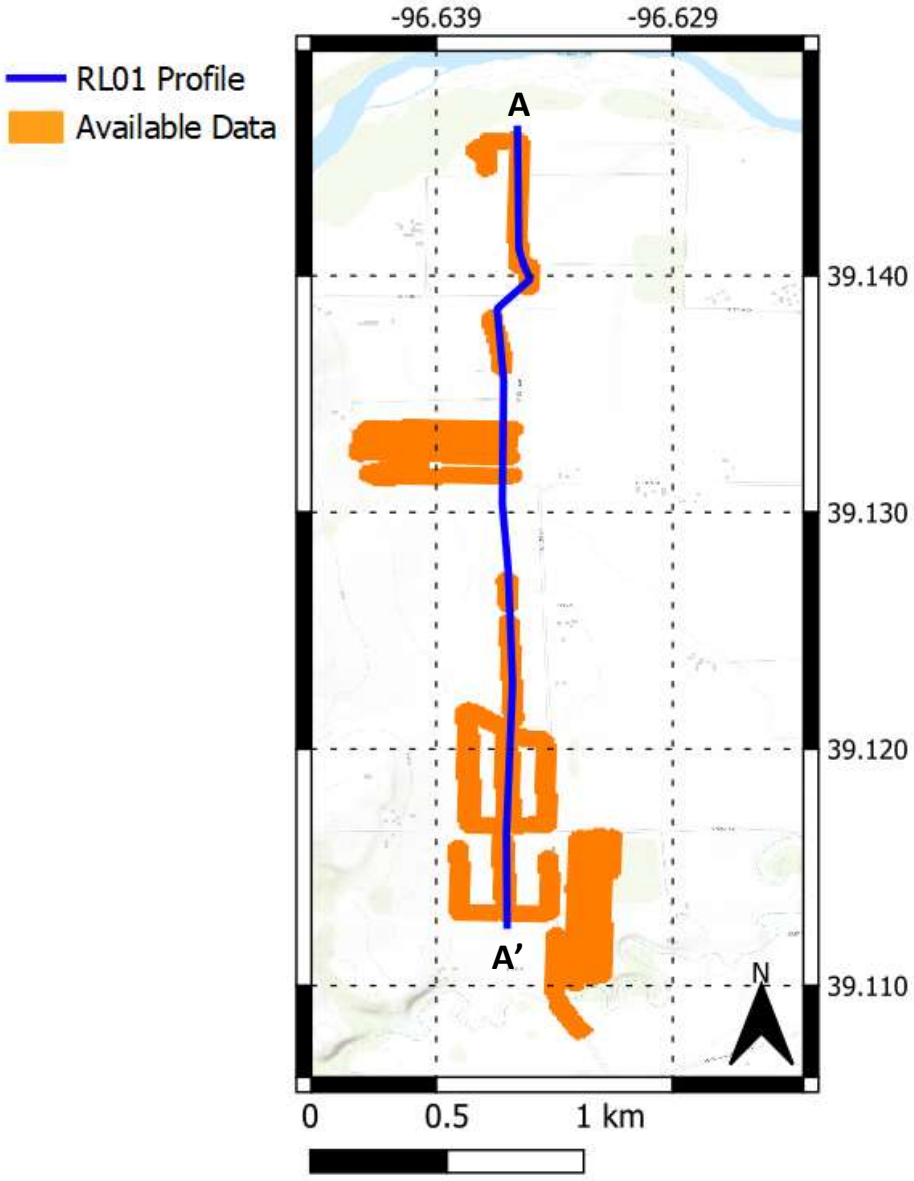

Figure 3.4 RL01 Available SCI data and Profile Line.

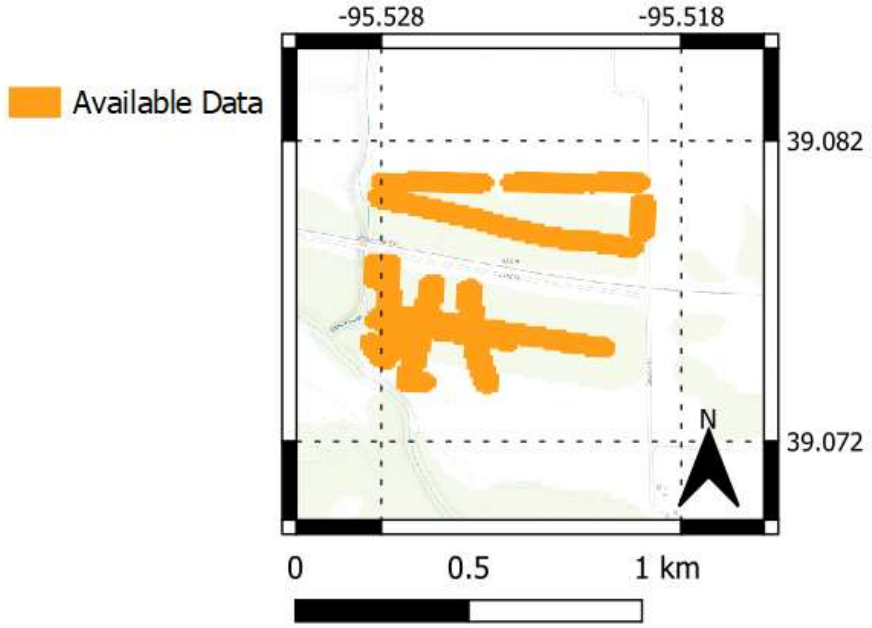

Figure 3.5 JF01 Available SCI data.

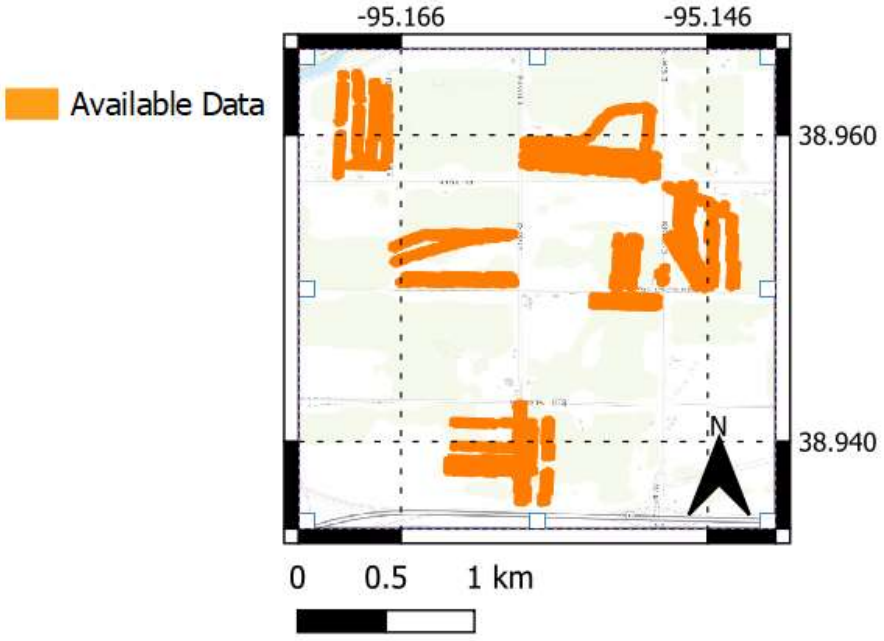

Figure 3.6 JF01 Available SCI data.

3.3. DIRECT PUSH ELECTRICAL CONDUCTIVITY

In conjunction with the tTEM data DPEC logs were collected at the survey locations. DPEC data was collected to compare with tTEM data. DPEC information is collected by advancing a small-diameter steel pipe with an electrical conductivity sensor at the end of the pipe (Butler et al., 2022). DPEC is commonly used in subsurface investigations as it has a very fine vertical resolution of 0.02 meters (Schulmeister et al., 2003). The fine resolution provided by DPEC reveals information about hydrostratigraphy and for the survey locations the distribution of coarse versus fine materials (Schulmeister et al., 2003). To compare the DPEC with tTEM, the DPEC data was resampled to tTEM SCI resolution. DPEC is known for highly detailed and accurate results at a defined location, and is used to justify tTEM results. We note, however, that the spatial footprint of DPEC data (tens of cm) is much smaller than that of the tTEM (~10 m), making exact comparisons between the two datasets infeasible. However, qualitative comparisons between trends observed in both datasets serves as a validation of the tTEM data.

3.4. RESISTIVITY – LITHOLOGY RELATIONSHIP

The resistivity-lithology relationship was determined using a method utilized in Knight et. al (2018). The method uses systems of equations to solve for resistivity of each user defined lithology type. For this study, it was determined three lithology types would be used based off 31 lithology well logs used in the study. The three lithology types are fine grained, mixed grained, and coarse grained. All data used for interpretation was below the water table. This was determined by using Kansas Geological Survey

continuous water level logs for each survey location. The resistivity-lithology method involved taking an SCI modeled resistivity profile pixel nearest to a lithology log and separating the SCI pixel into ratios based off lithology type. This process is done to all 31 lithology logs based on their location to the profiles and then combined into a list. The resulting lists comprise of a ratio of each lithology type along with the resistivity pixel values, providing three unknowns with one known value per modeled resistivity pixel. Combining all lithology well logs with this process, systems of equations can be used to solve for the resistivity value of each defined lithology type. Figure 3.7 depicts this process visually. Equation 1 outlines this process, where ρ_{tTEM} represents the resistivity value of each modeled resistivity pixel, t_{tTEM} is the thickness of each individual modeled resistivity pixel, $t_{a,b,c}$ is the thickness of each material type dependent on the lithology log from each well used to obtain ratios of the tTEM pixel over lithology type, and $\rho_{a,b,c}$ is each unknown resistivity value to be found using systems of equations.

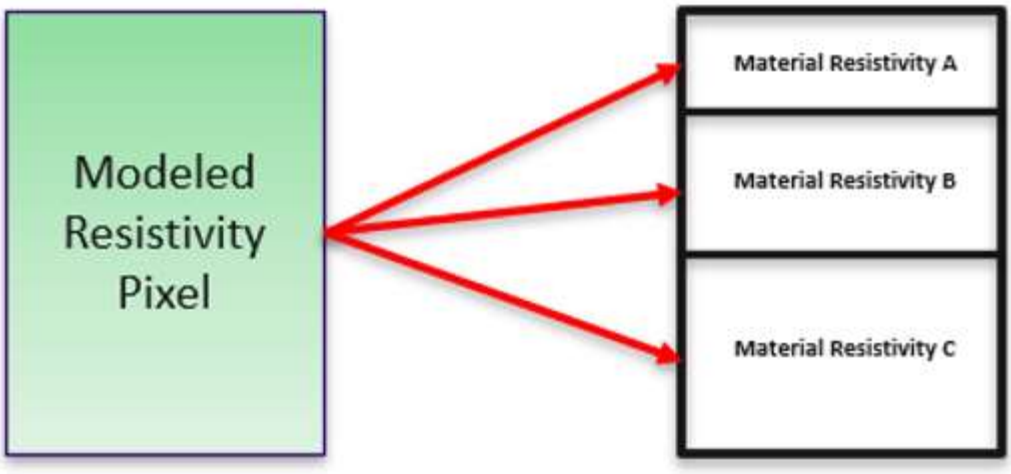

Figure 3.7 Resistivity-Lithology concept.

$$\frac{1}{\rho_{tTEM}} = \left(\left(\frac{t_{fine}}{t_{tTEM}}\right)\left(\frac{1}{\rho_{fine}}\right) + \left(\frac{t_{medium}}{t_{tTEM}}\right)\left(\frac{1}{\rho_{medium}}\right) + \left(\frac{t_{coarse}}{t_{tTEM}}\right)\left(\frac{1}{\rho_{coarse}}\right)\right) \quad (1)$$

Once the modeled resistivity pixel data was organized with corresponding unknown lithology resistivity ratios, all data was combined into a list to solve for lithology resistivity with systems of equations. To ensure a normal distribution of data, bootstrapping was conducted 1000 times, taking 100 samples with replacement of the organized data, then solving for resistivity of each lithology type each time.

3.5. KERNEL DENSITY ESTIMATION

To view the resistivity-lithology results, a new method was needed to view the distribution of fine, medium, and coarse material resistivity samples as there is considerable overlap of the range of values between materials. Kernel Density Estimation (KDE) is a method for visualizing the distribution of data, similar to a histogram (Silverman, 1986). In order for KDE to be implemented, the data must be a normal distribution. Fortunately, the results from the resistivity-lithology bootstrap analysis are normally distributed. The KDE equation is outlined in equation 2 where *K* is a kernel function (non-negative function), *h* is the bandwidth of each kernel, and *x* is a sample in a distribution of data (Silverman, 1986).

$$\widehat{f_h}(x) = \frac{1}{nh}\sum_{i=1}^{n} K\left(\frac{x-x_i}{h}\right) \quad (2)$$

The bandwidth parameter and kernel function used to analyze data are important variables in the overall shape of the function. A kernel function is the overall shape of each plotted data point. For this analysis, a gaussian kernel was used as it displays well with the normal distribution in the data. Bandwidth selection is a more quantitative

selection process, as small values of bandwidths lead to poor interpretability of the KDE, while large bandwidths lead to over interpretability of the KDE, which could miss important relationships within the data (Silverman, 1986). Because of this issue, a standardized approximation for bandwidth has been found based on the number of samples used in the analysis commonly referred to as Silverman and Scott's rule of thumb. Equation 3 outlines this relationship, where σ is the standard deviation and n is the number of samples used in the KDE analysis. Note that with the larger the sample size, the smaller the bandwidth. This equation is specifically for gaussian kernels.

$$h = 1.06\sigma n^{-1/5} \tag{3}$$

Figure 3.8 outlines different kernel function shapes, and Figure 3.9 outlines how the kernels are plotted and then stacked together to form the overall KDE.

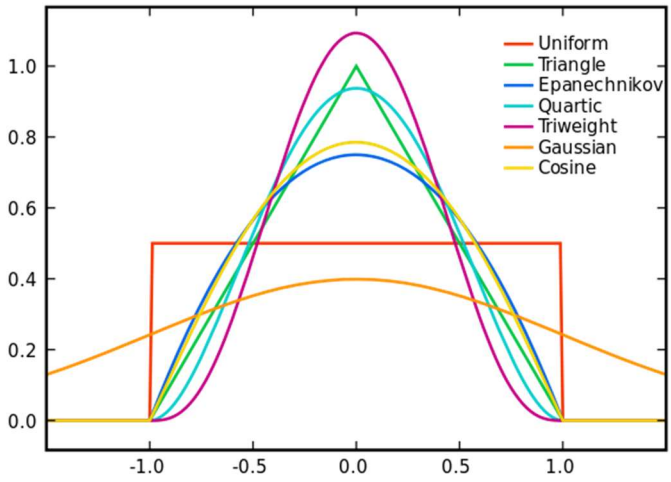

Figure 3.8 Kernel Shapes (Amberg, 2008).

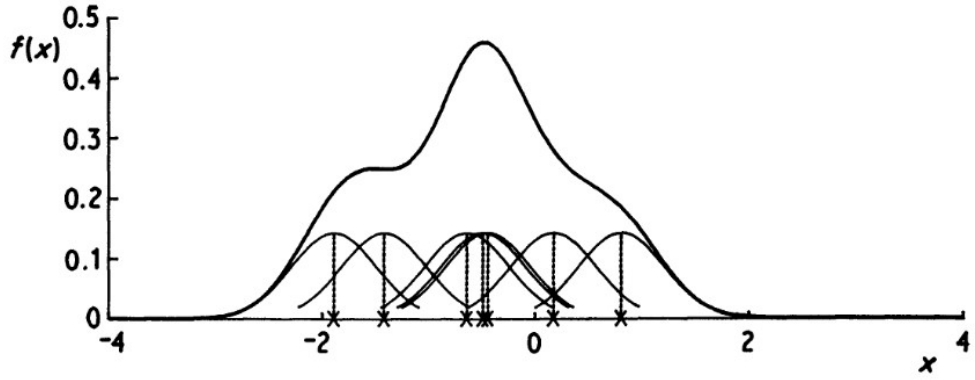

Figure 3.9 KDE Line with Individual Plotted Kernels (Silverman, 1986).

From equation 2 the overall function is approximately a smoothed version of the true density, obtained by combining f with the kernel scaled by the bandwidth (Silverman, 1986). This can be seen in Figure 4.8, where the resulting bootstrapped resistivity-lithology data is plotted by grain type with histograms, and the KDE curves are plotted around the distribution.

3.6. BEDROCK DELINEATION

From the resistivity-lithology analysis, three grain texture ranges and distributions were found. This analysis was conducted where data was available, which is above the soil-bedrock interface. This depth was approximately 25 meters at all locations, which leaves a considerable amount of useful tTEM data left for interpretation for bedrock delineation. Using the refusal depths of the 31 wells used in the resistivity-lithology analysis and DPEC refusal depths, an interpolated quadratic line (Refusal Depth Line, or RDL) was created for both WB01 and RL01 profiles. The standard deviation of tTEM SCI model values were then found below the RDL at both locations, which was added to

the average value of assumed bedrock pixels (40-55 meters in depth). Equation 4 outlines this function, where σ is the standard deviation below the RDL. The standard deviation below the refusal depth was added to the average bedrock value to account for the smooth inversion, where the SCI inversion would likely underestimate the soil-bedrock interface.

$$Bedrock\ Value = \sigma_{RDL} + AVG_{40-55m} \quad (4)$$

To delineate the bedrock, any pixels below the interpolated bedrock estimate from drilled wells that fell within the range of resistivity values described above was assigned to the bedrock category.

4. RESULTS & DISCUSSION

4.1. RESISTIVITY PROFILES

From the SCI inversions, two resistivity profiles were created. These include WB01 at Wamego, Kansas and RL01 at Manhattan, Kansas. There are shown in Figures 4.1 and 4.2.

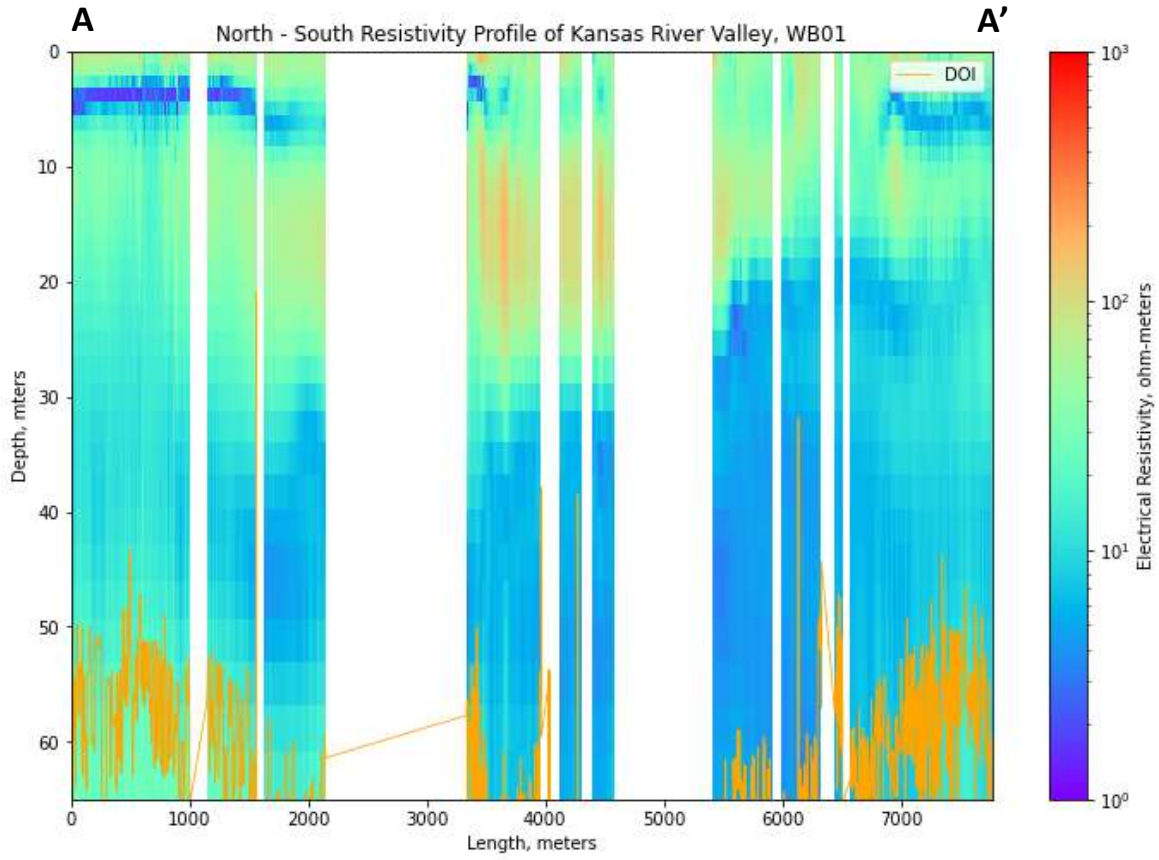

Figure 4.1 Resistivity Profile of WB01 at Wamego.

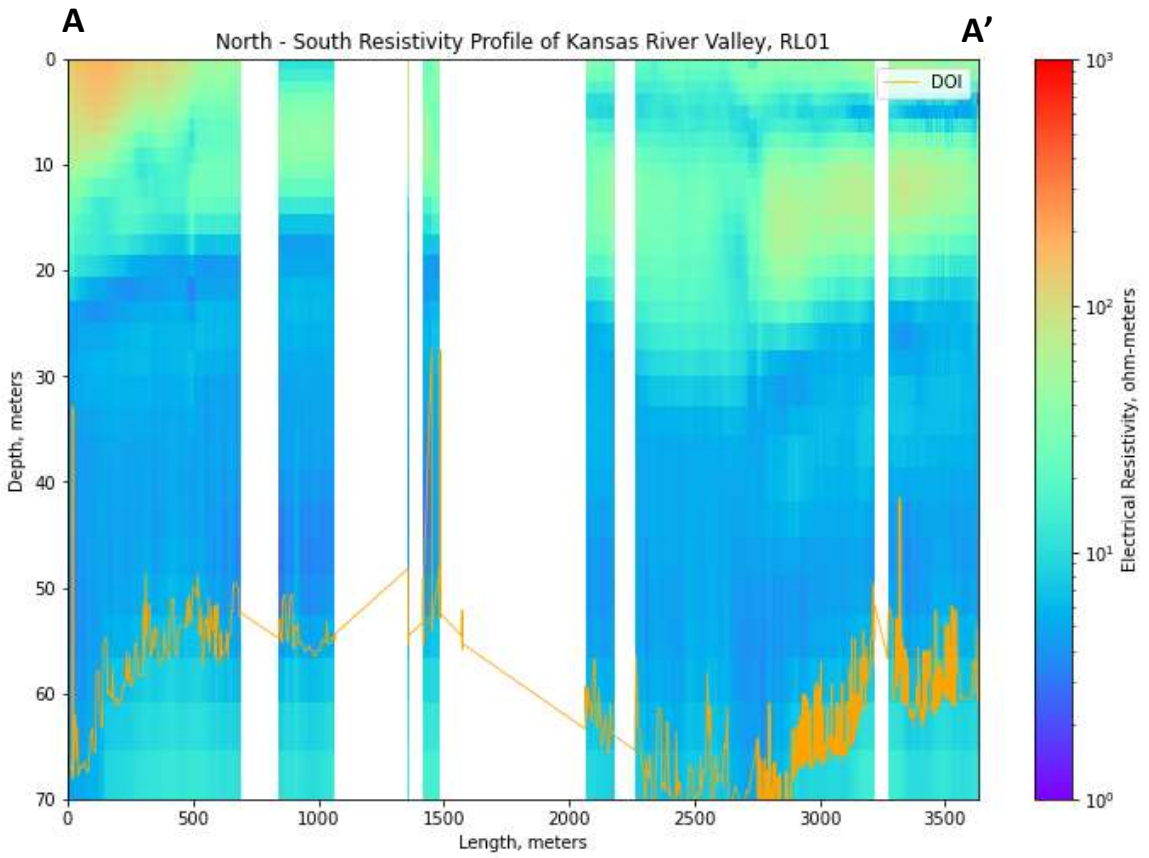

Figure 4.2 Resistivity Profile of RL01 at Manhattan.

From the resulting resistivity profiles, some general characteristics of the KRAA can start to be assumed. The conductive shale bedrock can be seen easily at RL01 and for a majority of WB01. Areas of high resistivity are also the areas most near the Kansas River, indicating alluvial deposition of large grain material. There is also a small conductive unit near the surface at approximately 5 meters in depth at both locations that end near the Kansas River for both locations. While these two locations are approximately 40 kilometers away, they show very strong similarities in overall structure as shown in the resistivity profiles.

The DOI can be seen in both Figures as well, where the SCI begins to converge back to the initial 40 Ohm-meter model past the line. It is suspected that the DOI at WB01 is less than RL01 because of the small very highly conductive unit at approximately 5 meters absorbing large amounts of signal. This can be shown in WB01, as the conductive unit ends the DOI increases. The DOI at RL01 follows the slight undulations in the conductive bedrock very well.

4.2. DIRECT PUSH ELECTRICAL CONDUCTIVITY – tTEM RELATIONSHIP

The tTEM data used in this study uses the smooth SCI model, which has smooth transitions from one pixel to the next. The smooth SCI inversion can take 1-3 pixels to fully transition to the next resistivity unit. When compared with the fine resolution of DPEC data, there is a large deviation between the DPEC and tTEM data. To improve the qualitative correlation between the tTEM and DPEC data, the DPEC data was resampled to the resolution of the tTEM SCI pixels. Qualitatively, the relationship appears to trend similarly. Quantitatively, the results show a poor relationship. Figure 4.3 outlines the correlation between tTEM and DPEC.

For the TEM method, the current system signal diffuses downward and outward (Foged & Christiansen, 2019). For a central loop TEM system, the footprint is circular, and for a TEM sounding the radius of the footprint is approximately twice the depth (Foged & Christiansen, 2019). The tTEM uses an off-set configuration, but except for the very shallow subsurface, the footprint is near-circular (Foged & Christiansen, 2019). Because of this the tTEM footprint is much larger compared to the very limited area surveyed using DPEC. The resulting tTEM data contain an average resistivity of the

surrounding material. When compared to the DPEC, will result in differences between the two datasets. In the alluvial setting of the KRAA, this difference can be amplified by the depositional variability of alluvial deposits. Figure 4.4 and 4.5 depicts the DPEC logs resampled at SCI intervals overlaying the tTEM resistivity profiles at both WB01 and RL01.

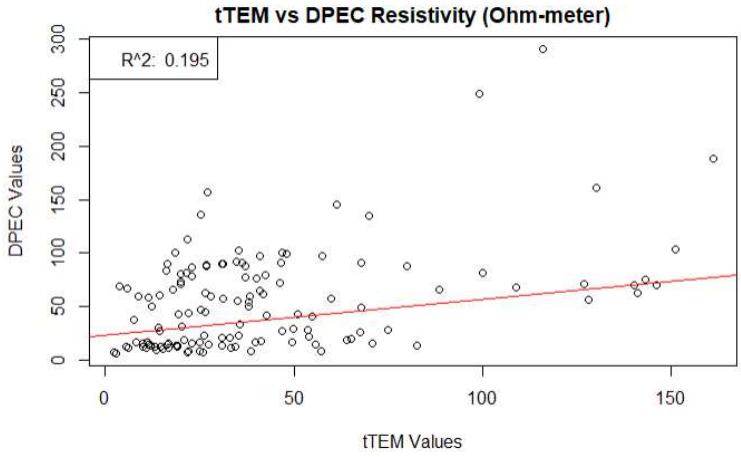

Figure 4.3 tTEM versus DPEC Correlation.

In spite of the difference in footprint between these two datasets, both show an extensive low-resistivity layer in the near-surface over much of the profiles shown in Figures 4.4 and 4.5. The DPEC logs show a thicker low-resistivity layer than the tTEM inversion results. This difference could be due to the non-uniqueness of tTEM inversions, where multiple realizations may fit the observed data equally well. Future work could use forward models to investigate multiple geologic scenarios that could fit the observed dB/dt data equally well to determine if some misfit is related to the inversion of tTEM data.

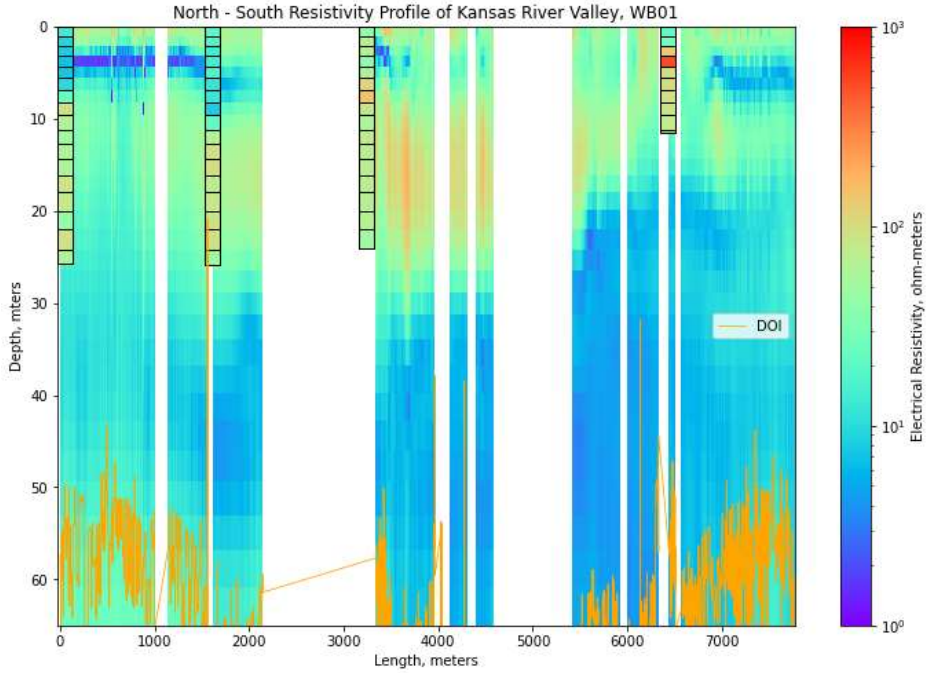

Figure 4.4 Resistivity Profile with DPEC logs at WB01.

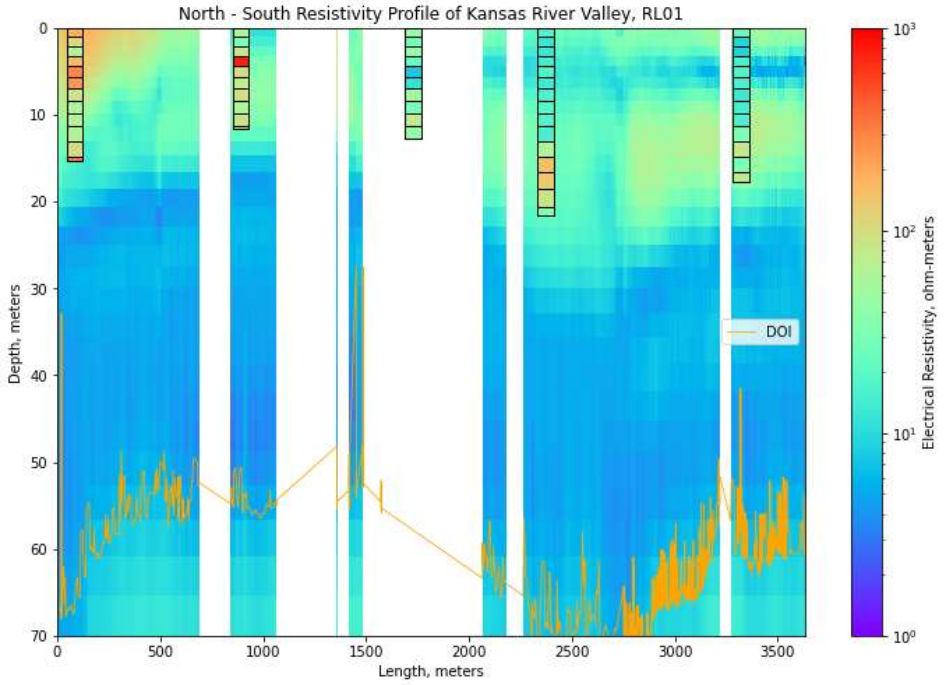

Figure 4.5 tTEM Resistivity Profile with DPEC logs at RL01.

4.3. LITHOLOGY WELLS

The lithology wells, along with their associated texture types, were plotted to view both how well lithology texture trends with the resistivity profiles but also to view refusal depth. From Figures 4.6 and 4.7, it can be seen a general trend is followed by the lithology wells, where there is a qualitative correlation between texture type and resistivity. It can also be observed that the refusal depth of the DPEC logs and lithology wells both tend to end approximately 1-3 pixels above the low resistivity pixels assumed to be the shale bedrock. This is likely due to the smooth SCI inversion, and is why the standard deviation below refusal depth was added to the average low-resistivity bedrock SCI pixels.

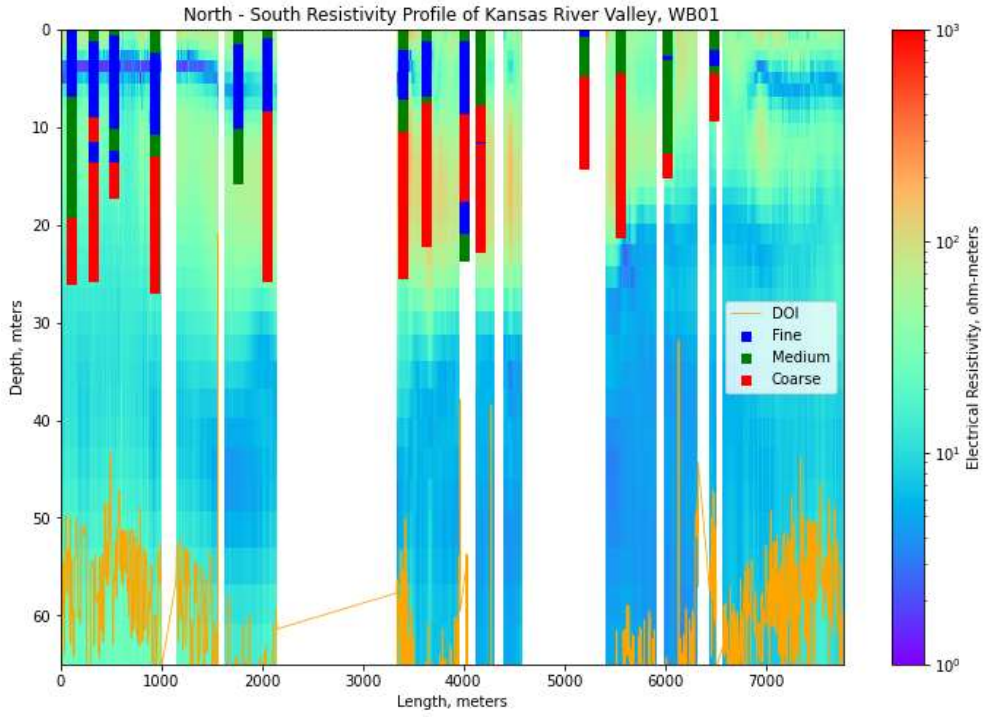

Figure 4.6 tTEM Resistivity Profile with Lithology Wells at WB01.

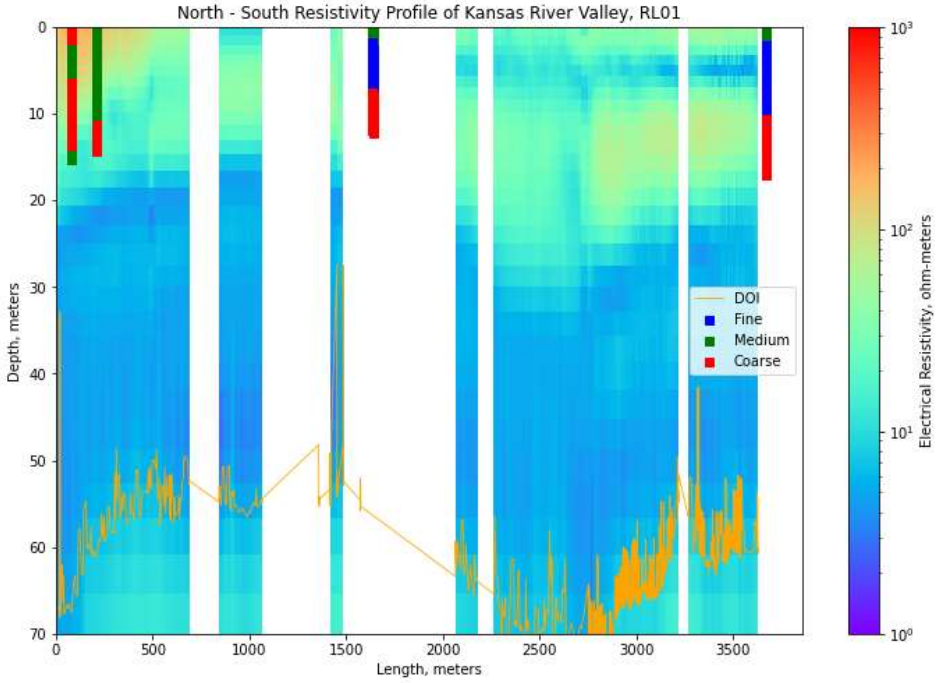

Figure 4.7 tTEM Resistivity Profile with Resistivity Wells at RL01.

4.4. RESISTIVITY – LITHOLOGY RELATIONSHIP

The table 4.1 contains the resistivity-lithology results of the bootstrap analysis.

Table 4.1 Resistivity Lithology Relationship.

Lithology Type	Minimum Resistivity (Ohm-Meter)	Maximum Resistivity (Ohm-Meter)	Median Resistivity (Ohm-Meter)
Fine Grained	13	39	22
Mixed Grained	24	52	35
Coarse Grained	38	67	52

From the analysis, it can be concluded that below the water table at these locations, any value from 0-39 Ohm-meters is fine grained material with some overlap of

mixed grained materials at the higher values in this range. Values of 24-52 Ohm-meters are mixed grained, with some overlap of fine-grained materials at the lower end of this range and overlap of coarse-grained materials at the upper end of this range. Coarse-grained material resistivity values are from 38 Ohm-meters to the maximum resistivities found below the water table.

To better visualize these results, the bootstrapped data was plotted into histograms and KDE was then performed and plotted as well as shown in Figure 4.8. The resulting KDE results are shown in Table 4.2.

From the KDE results, it can be shown the data used in the analysis was a normal distribution. It can also be determined that the resistivity-lithology analysis was successful in obtaining well separated results and results we would expect to see based on the expected resistivity of each texture.

Table 4.2 KDE Results.

Lithology Type	Minimum Resistivity (Ohm-Meter)	Maximum Resistivity (Ohm-Meter)
Fine Grained	0	29
Mixed Grained	30	44
Coarse Grained	45	∞

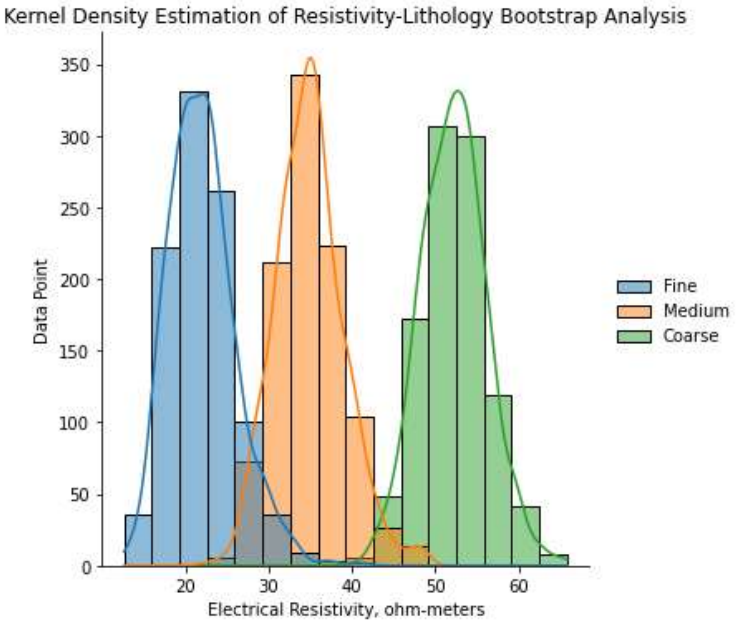

Figure 4.8 KDE Results.

Using the KDE results and the bedrock delineation process, texture profiles of the subsurface could then be created. From Figures 4.9 and 4.10, it can be concluded that near the Kanas River large amounts of coarse grained alluvial material is present. Once away from the Kansas River, smaller deposits can be found, possibly where the Kansas River could have meandered or from various streams that feed the Kansas River. Approximately a little over half of the data collected contained bedrock readings, which was plotted with refusal depth of both lithology and DPEC data. The general structure of the KRAA can therefore be deducted to be pockets of alluvial material surrounded by fine grained material, bounded by a shale bedrock.

From the resistivity-lithology results, resistivity information collected could then be interpreted to grain texture. Using the SCI sky view 1-meter rasters, grain texture can

be found over a large area. Using these interpreted results, areas of possible high producing wells could then be found.

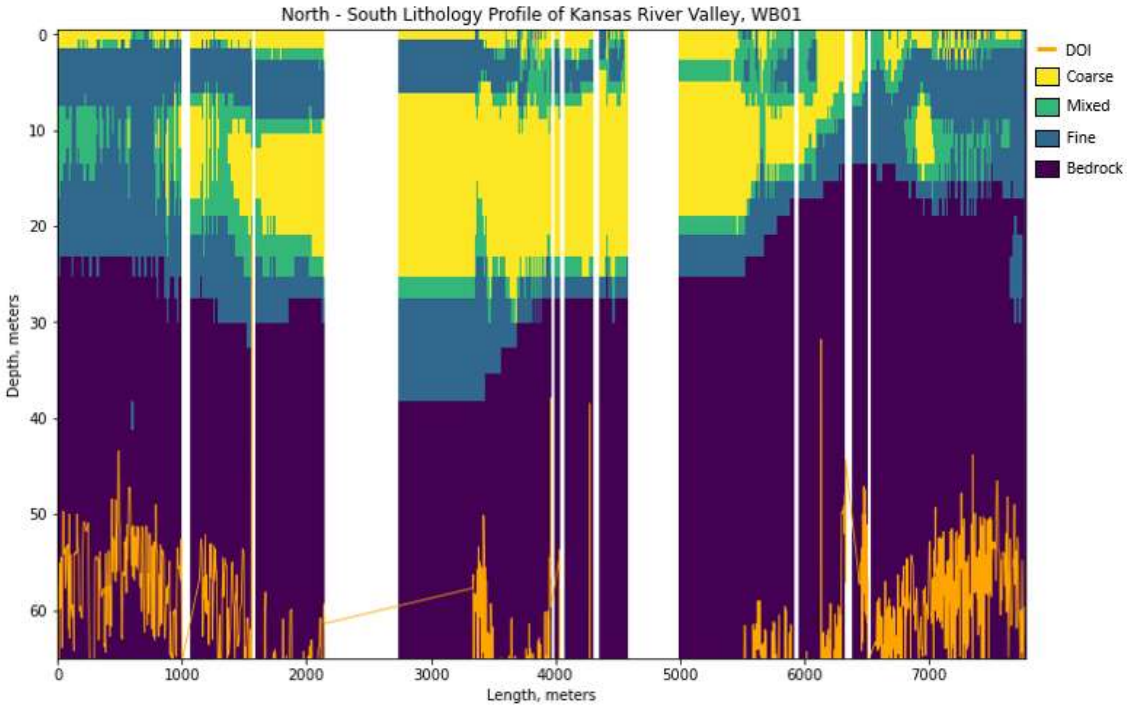

Figure 4.9 Subsurface Texture Profile of WB01 at Wamego.

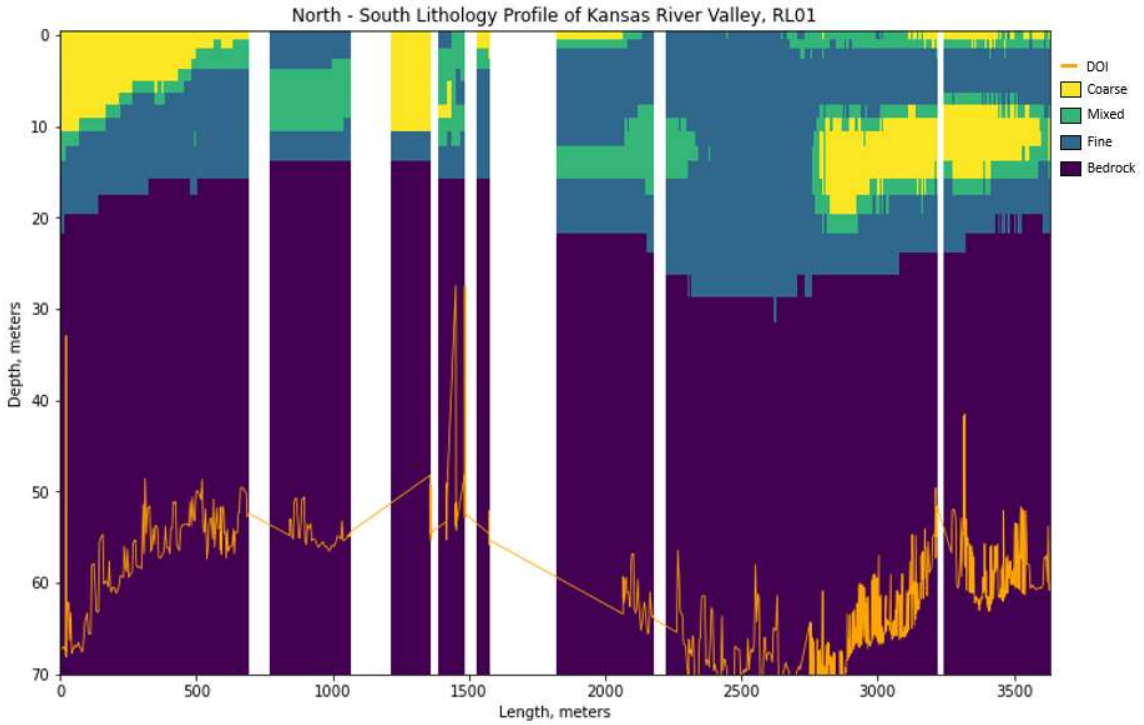

Figure 4.10 Subsurface Texture Profile of RL01 at Manhattan.

5. CONCLUSION AND RECCOMENDATIONS

The results of this work provide a detailed characterization of the KRAA that would not be possible without the use of the tTEM system. The tTEM system provides large amount of spatial data, where traditional methods such as interpolating between well logs, which would provide inconsistencies in an alluvial system such as the KRAA. The resulting resistivity-lithology analysis conducted resulted in a strong relationship between grain texture size and resistivity, which was shown through KDE to provide high quality subsurface grain texture profiles. Refusal depths of DPEC and lithology wells in the region resulted in characterization of the soil-bedrock interface. Using the subsurface grain texture profiles, the KRAA could then be characterized to have alluvial deposits underlain by a shale bedrock.

While the results in this study are believed to be accurate, there are sources of error. Comparing the DPEC data to tTEM data showed qualitative agreement as well as significant differences in thickness of various units. The poor quantitative relationship is likely due to the smooth SCI inversion of the tTEM data and the overall footprint of the tTEM system when compared to DPEC in an alluvial setting. The footprint of the tTEM system likely missed small pockets of highly resistive materials where the DPEC could detect these smaller units, but at a much smaller spatial resolution.

Recommendations to this study would be to find an in-depth analytical solution to map conductive bedrock more effectively than what was used in this study. The tTEM data in this study mapped the conductive shale bedrock very well qualitatively, but with the smooth inversion, provided error in exactly where this boundary is located. Refusal

depths from wells in the area provided in field measurements on where bedrock is actually located, which the tTEM results expanded on and defined a larger spatial area. While the bedrock mapped in this study appears to qualitatively match with the refusal depths and tTEM resistivity profiles, there is no real error metric on how well the process used in this study defines the soil-bedrock boundary. This recommendation would also apply to regions where there is resistive bedrock

BIBLIOGRAPHY

Amberg, B. (2008, February 12). *A range of different kernels*. Wikimedia Commons. https://commons.wikimedia.org/wiki/File:Kernels.svg

Auken, E., Foged, N., Larsen, J. J., Lassen, K. V. T., Maurya, P. K., Dath, S. M., & Eiskjær, T. T. (2019). tTEM — A towed transient electromagnetic system for detailed 3D imaging of the top 70 m of the subsurface. *GEOPHYSICS*, *84*(1), E13–E22. https://doi.org/10.1190/geo2018-0355.

Behroozmand, A. A., Auken, E., & Knight, R. (2019). Assessment of Managed Aquifer Recharge Sites Using a New Geophysical Imaging Method. *Vadose Zone Journal*, *18*(1), 1–13. https://doi.org/10.2136/vzj2018.10.0184

Butler, J., Reboulet, E., Knobbe, S., Bohling, G., Voss, J., & Wilson, B. (2022). Kansas Geological Survey Kansas River Alluvial Aquifer Index Well Program: June 2020 to May 2022 Report. *Jefferson County Index Well*, *2*(JF02). https://www.kgs.ku.edu/Publications/OFR/2022/OFR2022-6/OFR2022-6.pdf

Foged, N., & Christiansen, A. V. (2020, August). *Guideline and standards for tTEM data collection, processing, and inversiton* [Review of *Guideline and standards for tTEM data collection, processing, and inversiton*]. Aarhus University HydroGeophysics Group; Aarhus University. https://hgg.au.dk/fileadmin/HGGfiles/Reports/Guide_tTEM.pdf

Foged, N., & Christiansen, A. V. (2019, November). *The tTEM System System validation and comparison with PACES and ERT* [Review of *The tTEM System System validation and comparison with PACES and ERT*]. Aarhus University HydroGeophysics Group; Aarhus University. https://hgg.au.dk/fileadmin/HGGfiles/Reports/tTEM_Validation_2019.pdf

Goebel, M., & Knight, R. (2021). Recharge site assessment through the integration of surface geophysics and cone penetrometer testing. *Vadose Zone Journal*, *20*(4). https://doi.org/10.1002/vzj2.20131

Knight, R., Smith, R., Asch, T., Abraham, J., Cannia, J., Viezzoli, A., & Fogg, G. (2018). Mapping Aquifer Systems with Airborne Electromagnetics in the Central Valley of California. *Groundwater*, *56*(6), 893–908. https://doi.org/10.1111/gwat.12656

Reynolds, J. M. (2011). *An introduction to applied and environmental geophysics*. Wiley-Blackwell.

Schamper, C., Pedersen, J. B., Auken, E., Christiansen, A. V., Vittecoq, B., Deparis, J., Jaouen, T., Lacquement, F., Nehlig, P., Perrin, J., & Reninger, P.-A. . (2013). Airborne Transient EM Methods and Their Applications for Coastal Groundwater Investigations. *Groundwater in the Coastal Zones of Asia-Pacific*, 121–153. https://doi.org/10.1007/978-94-007-5648-9_7

Schulmeister, M. K., Butler, J. J., Healey, J. M., Zheng, L., Wysocki, D. A., & McCall, G. W. (2003). Direct-Push Electrical Conductivity Logging for High-Resolution Hydrostratigraphic Characterization. *Ground Water Monitoring & Remediation*, *23*(3), 52–62. https://www.academia.edu/33675901/Direct_Push_Electrical_Conductivity_Logging_for_High_Resolution_Hydrostratigraphic_Characterization6

Silverman, B. W. (1986). Density Estimation for Statistics and Data Analysis. In *Google Books*. CRC Press. https://books.google.com/books?printsec=frontcover&vid=ISBN0412246201&vid=LCCN85021347#v=onepage&q&f=false

Viezzoli, A., Auken, E., & Munday, T. (2009). Spatially constrained inversion for quasi 3D modelling of airborne electromagnetic data – an application for environmental assessment in the Lower Murray Region of South Australia. *Exploration Geophysics*, *40*(2), 173–183. https://doi.org/10.1071/eg08027

Whittemore, D. O., Wilson, B., & Butler, Jr., J. J. (2019, July 8). *Kansas River Alluvial Aquifer: Water Use and Real-Time Monitoring* [Review of *Kansas River Alluvial Aquifer: Water Use and Real-Time Monitoring*]. Kansas Geological Survey. https://www.kgs.ku.edu/Hydro/Publications/2019/OFR19_18/index.html

VITA

Jonathon Daniel Voss received his B.S. in Geological Engineering in May 2021 from Missouri University of Science and Technology and received his M.S. in Geological Engineering from the University of Missouri of Science and Technology in December of 2022.